

Biology Contribution

Microsecond Pulsed Electric Fields: An Effective Way to Selectively Target and Radiosensitize Medulloblastoma Cancer Stem Cells



Mirella Tanori, PhD,* Arianna Casciati, PhD,*
Alessandro Zambotti, MD,* Rosanna Pinto, MD,*
Isabella Gianlorenzi, MD,† Alessandro Pannicelli, MD,‡
Paola Giardullo, PhD,* Barbara Benassi, PhD,* Carmela Marino, PhD,*
Mariateresa Mancuso, PhD,* and Caterina Merla, PhD*

*Division of Health Protection Technologies, Italian National Agency for Energy New Technologies and Sustainable Economic Development (ENEA), Rome, Italy; †Department of Ecological and Biological Sciences, University of Tuscia, Viterbo, Italy; and ‡Energy Efficiency Department, ENEA, Rome, Italy

Received Jul 7, 2020, and in revised form Oct 22, 2020. Accepted for publication Nov 12, 2020.

Purpose: Cancer stem cells constitute an endless reserve for the maintenance and progression of tumors, and they could be the reason for conventional therapy failure. New therapeutic strategies are necessary to specifically target them. In this context, microsecond pulsed electric fields have been selected to expose D283Med cells, a human medulloblastoma cell line resulted to be rich in cancer stem cells, and normal human astrocytes.

Methods: We analyzed in vitro different endpoints at different times after microsecond pulsed electric field exposure, such as permeabilization, reactive oxygen species generation, cell viability/proliferation, cell cycle, and clonogenicity, as well as the expression of different genes involved in cell cycle, apoptosis, and senescence. Furthermore, the response of D283Med cells exposed to microsecond pulsed electric fields was validated in vivo in a heterotopic mouse xenograft model.

Results: Our in vitro results showed that a specific pulse protocol (ie, 0.3 MV/m, 40 μ s, 5 pulses) was able to induce irreversible membrane permeabilization and apoptosis exclusively in medulloblastoma cancer stem cells. In the surviving cells, reactive oxygen species generation was observed, together with a transitory G2/M cell-cycle arrest with a senescence-associated phenotype via the upregulation of GADD45A. In vivo results, after pulsed electric field exposure, demonstrated a significant tumor volume reduction with no eradication of tumor mass. In conjunction, we verified the efficacy of electric pulse pre-exposure followed by ionizing irradiation in vivo to enable complete inhibition of tumor growth.

Corresponding authors: Mariateresa Mancuso, PhD and Caterina Merla, PhD; E-mail: mariateresa.mancuso@enea.it or caterina.merla@enea.it

Mirella Tanori and Arianna Casciati contributed equally to this paper.

This project has received funding from the European Union's Horizon 2020 research and innovation program under grant agreement no. 737164 SUMCASTEC. It was also partially supported by grant from MIUR (Italian Ministry of University and Research) "ENEA 5 \times Mille" (Young investigator Project: New therapeutic strategies for the treatment of cancer)

to M. Tanori and by grant no. 20314 from the Fondazione AIRC per la Ricerca sul Cancro (NANOCROSS project) to M. Mancuso.

Disclosures: M.T., A.C., A.Z., R.P., C.M., M.M., and C.M. are inventors on pending patent related to the work. The authors declare no other conflicts of interest.

Data availability statement: All data generated and analyzed during this study are included in this published article and are available upon reasonable request to the corresponding author.

Supplementary material for this article can be found at <https://doi.org/10.1016/j.ijrobp.2020.11.047>.

Conclusions: Our data reveal novel therapeutic options for the targeting of medulloblastoma cancer stem cells, indicating nonionizing pulsed electric field pre-exposure as an effective means to overcome the radioresistance of cancer stem cells. © 2020 The Authors. Published by Elsevier Inc. This is an open access article under the CC BY-NC-ND license (<http://creativecommons.org/licenses/by-nc-nd/4.0/>).

Introduction

In recent years, pulsed electric fields of high amplitude (from a few to hundreds of kV/m) and short duration (from a few milliseconds to few microseconds) have emerged as a very powerful physical agent determining cell electroporation (or electroporation).¹ Electroporation is a biophysical phenomenon in which cell membranes exhibit increased permeability to ions and macromolecules.^{1,2} It has multiple applications in oncologic treatments as, for example, in electrochemotherapy (ECT).^{3,4} ECT enables microsecond pulsed electric fields (μ sPEF) to reversibly permeate cell membranes with chemotherapeutic drugs (eg, bleomycin), leading to an enhancement of their effects by more than 1000 times. Owing to its effectiveness and safety for patients, this clinical approach is spreading rapidly and is now widely used in European and worldwide hospitals for the treatment of superficial and deep tumors.^{5,6}

Another emerging use of μ sPEF in the clinic concerns so-called irreversible electroporation (IRE) and high-frequency irreversible electroporation (H-FIRE), in which repeated monopolar and/or bipolar electric pulses are used, causing direct cell death via the loss of cell homeostasis produced by hydrophilic pores induced in cellular membranes.^{7,8} The nonthermal cell death induced by IRE or H-FIRE is beneficial in comparison with other technologies⁹ because it can save healthy critical structures in the surrounding treated area. Hence, IRE/H-FIRE are currently being evaluated in a range of veterinary and human clinical trials for malignancies in the liver, pancreas, prostate, kidney, and brain.¹⁰

Recently, all these therapeutic applications (ECT, IRE, and H-FIRE) appeared also extremely valuable for their immune system engagement by stimulating innate immunity through the induction of inflammatory cell death and in situ activation of an anti-inflammatory tumor microenvironment.^{11,12} These effects function to eliminate metastases and to promote tumor remission in the long term.¹³

In this context, another relevant opportunity associated with these electrically mediated therapies comes from the possibility to selectively target cancer stem cells (CSCs).¹⁴ CSCs are the malignant equivalent of normal somatic stem cells and are responsible, in tumorigenesis, for driving tumor growth, repopulation after injury, and metastasis spread.¹⁵ CSCs have been described as intrinsically resistant to standard radiation/chemotherapy owing to a complex mixture of genetic alterations, expression of multidrug resistant transporters, and protection exerted by particular microenvironmental niches.¹⁶ Therefore, targeting these

tumor-initiating cells is a powerful strategy to eliminate the cause of disease.¹⁵

This option is interesting for brain cancers, in which the presence of CSCs has been ascertained, explaining their extremely high recurrence and their fast regrowth rate.^{15,17} Indeed, next-generation therapies working effectively against brain CSCs alone and in combination with conventional oncologic approaches (eg, radiation therapy and chemotherapy) are greatly desired. Among brain cancers, pediatric ones are of special interest, being the leading cause of death in children and adolescents from 0 to 19 years old.¹⁸ Medulloblastoma (MB), a highly malignant primitive neuroectodermal tumor of the cerebellum, represents about 20% of all childhood primary tumors of the central nervous system.¹⁹

To test the potential efficacy of μ sPEF on MB CSCs, we analyzed different in vitro endpoints on D283Med cells, reportedly rich in CSCs,²⁰ and on a normal human astrocyte (NHA) primary cell line. We evaluated cell permeabilization and reactive oxygen species (ROS) production, cell viability, growth rate, cell cycle, and perturbation of molecular pathways. Clonogenic potential in vitro and in vivo tumor growth characterizations were also examined after μ sPEF exposure, alone and in combination with x-rays.

Globally, our results demonstrate selective and effective action of μ sPEF on MB CSCs, preserving normal cells. The combined treatment could be very promising and could lead to an overall future improvement of MB therapy, reducing the well-known consequences of radiation therapy on neurocognitive functions, particularly in children, for whom they represent a major harmful side effect of life-saving therapies.

Materials and Methods

Cell cultures

The human D283Med cell line (indicated as D283) was obtained from American Type Culture Collection (Manassas, VA). Cells (with doubling time of 52 hours) were routinely maintained in complete growth medium with Eagle's Minimum Essential Medium supplemented with 10% fetal bovine serum, 2 mM glutamine, and 100 U penicillin/0.1 mg/mL streptomycin. Primary culture of NHA and their optimized growth medium were purchased from Lonza (Switzerland). These cells were used in all experiments between passages 2 and 4.

Cell exposure to μ sPEF and ionizing radiation

Cells were exposed to electric fields via electroporation cuvettes (0.1-cm gap, Bio-Rad) connected to a pulse generator (Schaffner NSG504).^{21,22} The voltage pulse waveforms were monitored in real time via a Tektronix TDS5054B-NV oscilloscope and a high-voltage probe (LeCory PPE 5 kV). To maintain a fixed load of 50 Ω , cells were exposed at a concentration of 6×10^5 cells in 100 μ L of an artificial isotonic buffer as detailed by Davis et al.²¹ Cell viability in this buffer was tested with trypan blue assay. Cell viability greater than 90% is assured for more than 3 hours of cell suspension in the buffer.

Electric pulses of exponential shape were used in our experiments. Their amplitude and duration were maintained at 300 V (for an electric field of 0.3 MV/m) and 40 μ s at full width at half maximum, respectively. Cells were exposed to a different number of electric pulses (1, 3, and 5) to assess the threshold of reversible versus irreversible electroporation. The interpulse interval was equal to 1 Hz.

Cells and tumors were irradiated using a Gilardoni CHF 320 G x-ray generator (Gilardoni, Mandello del Lario, Lecco, Italy) operated at 250 kVp, 15mA, with HVL = 1.6 mm Cu (additional filtration of 2.0 mm Al and 0.5 mm Cu). The dose rate was 0.89 Gy/min at an irradiation distance of 67.7 cm.

Viability assays

Cell suspensions were mixed 1:1 with trypan blue dye, and accurate viability data were recorded with a LUNA-II cell counter (Logos Biosystem, France) at 0, 24, and 48 hours after the exposure. According to the manufacturer's instructions, a RealTime-Glo MT Cell Viability Assay (Promega, Italy) was also carried out to monitor cell viability in real time. Luminescence was quantified at 0, 24, and 48 hours after plating by a GloMax (Promega, Italy).

Flow cytometric analyses

Cell permeabilization

Membrane permeability was analyzed immediately after electric exposure ($T = 0$ hours) and 3 hours later ($T = 3$ hours). D283 cells and NHA were detached and resuspended in the electroporation buffer, and Yo-Pro-1 (Life Technologies, Italy, $\lambda_{\text{ex}} = 490$ nm, $\lambda_{\text{em}} = 510$ nm) was added at a concentration of 5 μ M.²³ Exposed cells were diluted in phosphate-buffered (1:5) and analyzed by flow cytometry ($T = 0$ hours) within 10 minutes from the exposure. To check permeabilization at $T = 3$ hours, exposed plated cells were stained and analyzed as described.

Using a FACS Calibur (BD Bioscience, Italy), forward (FSC-H) and side scatterings (SSC-H) were used to exclude cellular debris from the analysis and to gate the integer/healthy cells. Data were acquired using Cell Quest software and analyzed using FCS Express v.7 (De Novo, Italy).

Evaluation of ROS

Cells were stained with dihydroethidium (DHE) to measure ROS²⁴ immediately after the electric exposure ($T = 0$ hours) and 3 hours later ($T = 3$ hours). Cells were detached, washed, and labeled with 5 μ M DHE ($\lambda_{\text{ex}} = 518$ nm, $\lambda_{\text{em}} = 605$ nm) at 37°C in the dark for 20 minutes. After being washed, cells were resuspended in the electroporation buffer ready for μ sPEF treatment, and then they were analyzed by flow cytometry at $T = 0$ hours²⁵ (within 10 minutes of exposure).

To check ROS at $T = 3$ hours, exposed plated cells were detached, washed, labeled, and analyzed as previously described.

The mean fluorescence intensity was calculated for each sample as the ratio of the mean fluorescence value in the channel of the probe-labeled and sham-treated cells. Unstained samples (negative) were used to subtract the cell autofluorescence.

Cell cycle

In summary, about 1 million cells were fixed with cold 70% ethanol solution, vortexed, and incubated at 4°C. Harvested cells were centrifuged, and pellets were resuspended in propidium iodide (PI)/RNase staining buffer ($\lambda_{\text{ex}} = 490$ nm, $\lambda_{\text{em}} = 600$ nm, BD Biosciences). Cell cycle was analyzed at 24 hours from the exposure. Samples were analyzed by flow cytometry as previously described.

RNA isolation and RT2 Profiler PCR Array

RNA isolation from cells was performed with RNeasy Mini Kit (QIAGEN, Italy). After quantification, 0.5 μ g of total RNA was reverse transcribed with a High-Capacity cDNA Reverse Transcription Kit (Applied Biosystems). For quantitative comparison of cell cycle gene mRNA levels, real-time PCR was performed using Human Cell Cycle RT2 Profiler PCR Array (QIAGEN), and qPCR was carried out with StepOnePlus Real-Time PCR System (Applied Biosystems). Gene expression was related to the mean expression of all 5 housekeeping genes included in the array. Only Ct values <35 were included in the calculations. The $\Delta\Delta$ Ct quantitative method was used to normalize expression of the reference gene and to calculate the relative expression levels of target genes.²⁶

Pathway analyses

The pathway analyses were performed as described in previous work.²⁶ In the analyses, a cutoff of 2 was taken into account for deregulated genes.

Western blot

Cells were lysed with T-PER Reagent (Thermo Fisher Scientific) added with protease and phosphatase inhibitors; 30 μ g of proteins were loaded and separated by

SDS-PAGE. Proteins were electrotransferred to PVDF membranes using the Trans-Blot Turbo Transfer System (BIO-RAD Laboratories). After blocking, membranes were incubated with primary antibodies against GADD45A (Santa Cruz Biotechnology), p15 (Abcam), cleaved-caspase-3 (Abcam), and HSP70 (Sigma-Aldrich). Membranes were probed with appropriated HRP-conjugated secondary antibodies (Santa Cruz Biotechnology). Immunoreactive bands were visualized using Amersham ECL Prime WB detection reagent (GE Healthcare Europe). Images were acquired using Image 6 quant LAS 500 (GE Healthcare Europe), and densitometric analysis was performed using ImageJ software.

Clonogenic survival

Clonogenic cell survival was determined by colony formation assay. Appropriate cell numbers in the range of 100 to 3000 cells were seeded in 6-well plates pretreated with polylysine. Sham and pulsed cells were exposed to x-rays (0, 2, 5, and 8 Gy) 3 hours after seeding. After approximately 14 days, colonies were fixed with methanol and stained with crystal violet (0.5% in methanol 50%). Colonies consisting of >50 cells were counted. Surviving fractions were normalized by the plating efficiency of unirradiated controls.

In vivo xenograft models

Female NU/NU CD1 mice were purchased from Charles River Laboratories (Lecco) and housed in sterilized filter-topped cages kept in laminar flow isolators, fed with autoclaved food and water ad libitum, and maintained in a 12-hour light/dark cycle. MB cells (6×10^6) in Matrigel (BD Biosciences), with or without exposure to μ sPEF in vitro, were injected subcutaneously in mice at 6 to 8 weeks of age. Injection occurred within a maximum of 15 minutes from the exposure. Injected animals were monitored daily, and tumors were measured with a caliper twice a week. After 3 hours from injection, some groups of mice were irradiated; during the delivery of irradiations, mice were lightly anesthetized with 35 mg/kg of pentobarbital sodium, and the body was shielded with 4-mm thick lead plates to irradiate only the injected cells. Tumor dimension was estimated using the following formula: tumor volume = $(\text{length} \times \text{width})^2/2$. To evaluate differences in efficacy between treatment groups, the percentage of tumor growth inhibition (TGI) was calculated as $\text{TGI}(\%) = (\text{Vc} - \text{Vt})/(\text{Vc} - \text{Vo}) \times 100$, where Vc and Vt are the median of control (sham) and treated groups at the end of the study and Vo is at the start.^{27,28}

Animal studies were performed according to the European Community Council Directive 2010/63/EU and were authorized by the Italian Ministry of Health (n.80/2017-PR).

Statistical analysis

Results are expressed as mean of 3 biological replicates \pm standard error of the mean. All statistical tests were performed with GraphPad Prism software v.7 (GraphPad, CA). *P* values were determined using the 2-tailed *t* test (**P* < .05; ***P* < .01; ****P* < .001; and *****P* < .0001).

Results

PEF-5 exposure induces permeabilization and affects survival, proliferation, and ROS formation in CSCs

To evaluate μ sPEF's ability to induce cell membrane permeabilization, we used different numbers of pulses. Graphs in Figure 1A show the percentage of permeabilized D283 cells immediately (*T* = 0 hours) and 3 hours (*T* = 3 hours) after exposure to different numbers of electric pulses. The permeabilization increased proportionally to the number of pulses. It is shown that cell recovery after 3 hours from the exposure is highly impaired when 5 electric pulses are applied, suggesting this pulse number is a threshold for irreversible cell electroporation. This hypothesis is further confirmed by looking at the cell viability curves (Fig. 1B), in which high cell mortality is associated with the delivery of 5 electric pulses up to 72 hours postexposure. Using a reduced μ sPEF number (1 and 3), cell viability was not affected with respect to the sham. Therefore, this pulse protocol (0.3 MV/m, 40 μ s, 5 pulses [PEF-5]) inducing cell permeabilization and prolonged impairment of cell viability was adopted to characterize μ sPEF action on D283 cells. To investigate a possible selective effect of PEF-5 on MB CSCs, we also exposed NHA. We found a high number of permeabilized cells immediately after exposure. However, this phenomenon is transient; at 3 hours after exposure, the dye uptake markedly decreased (Fig. 1C). The trypan blue assay highlighted that pulsed NHA were resistant to this treatment, maintaining high viability at all tested time points (Fig. 1D). These results suggest that NHAs are characterized by a higher threshold for irreversible electroporation than D283 cells.

Electric pulses act as stressors for cell membranes. Hence, to defend themselves, exposed cells can generate ROS.²⁹ For this reason, we decided to evaluate ROS as an important second messenger in addressing cell fate.³⁰ DHE, assessed immediately after PEF-5 exposure, did not show any increase with respect to sham-exposed NHA and D283 cells; notably, a statistically significant ROS increase was observable after 3 hours from the electric exposure exclusively in D283 (Fig. 1E-G).

Cell membrane electropermeabilization, ROS increase, and high levels of cell death could have an important impact on cell proliferation rates. As shown in Figure 1H and 1I, exposure to PEF-5 induced a 7.3- or 7.9-fold lower

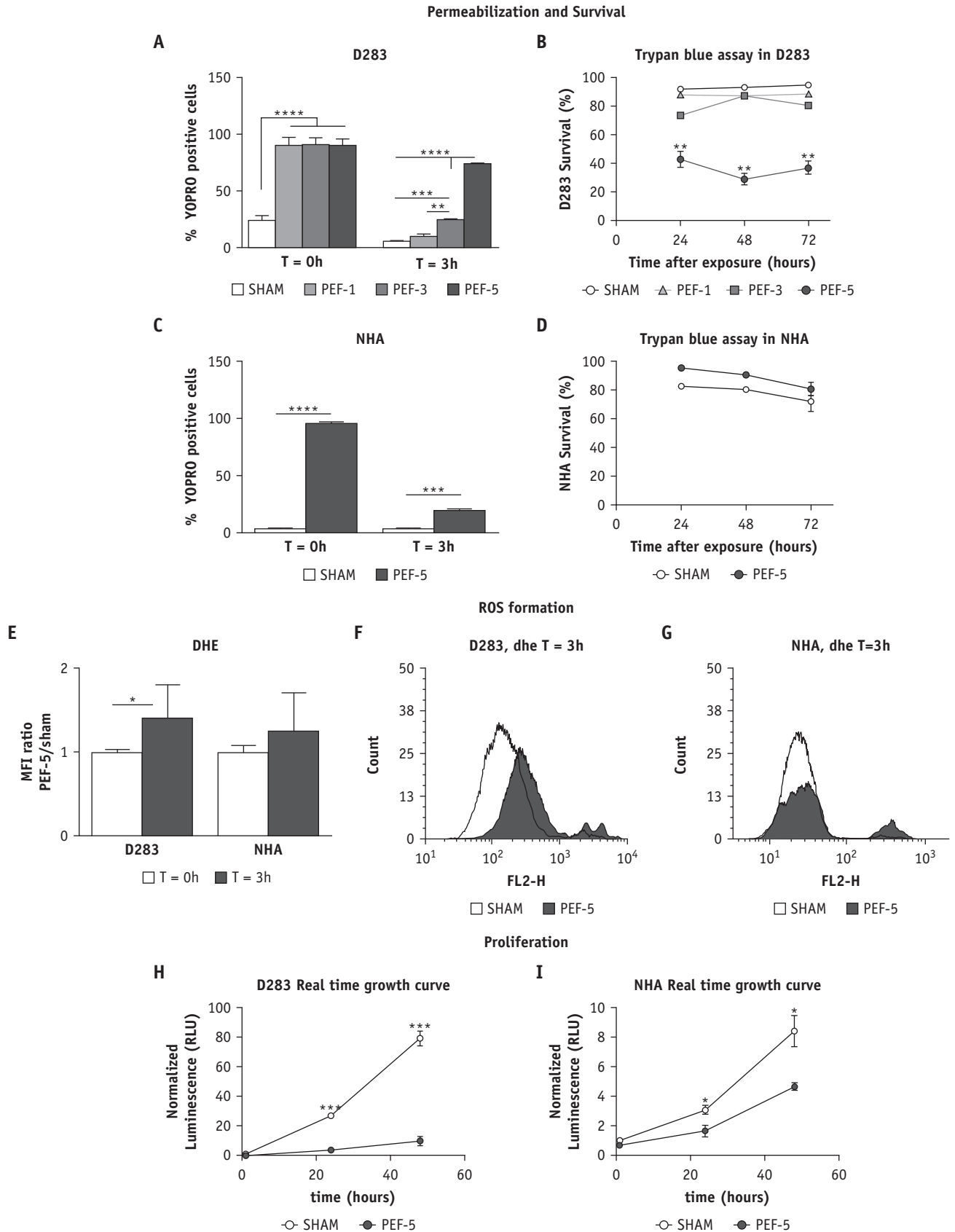


Fig. 1. Characterization of PEF-5 exposure on D283 and normal human astrocytes (NHA). Membrane permeabilization immediately and 3 hours postexposure in D283 (A and B) and NHA (C). Percent cell survival in D283 (D) and NHA (E) at 24 and 48 hours after exposure. Dihydroethidium (DHE) mean fluorescence intensity ratio in D283 (E and F) and NHA (E and G) immediately and 3 hours postexposure. Cell viability in D283 (H) and NHA (I) at 0, 24, and 48 hours after exposure. Data are normalized to sham-treated cells.

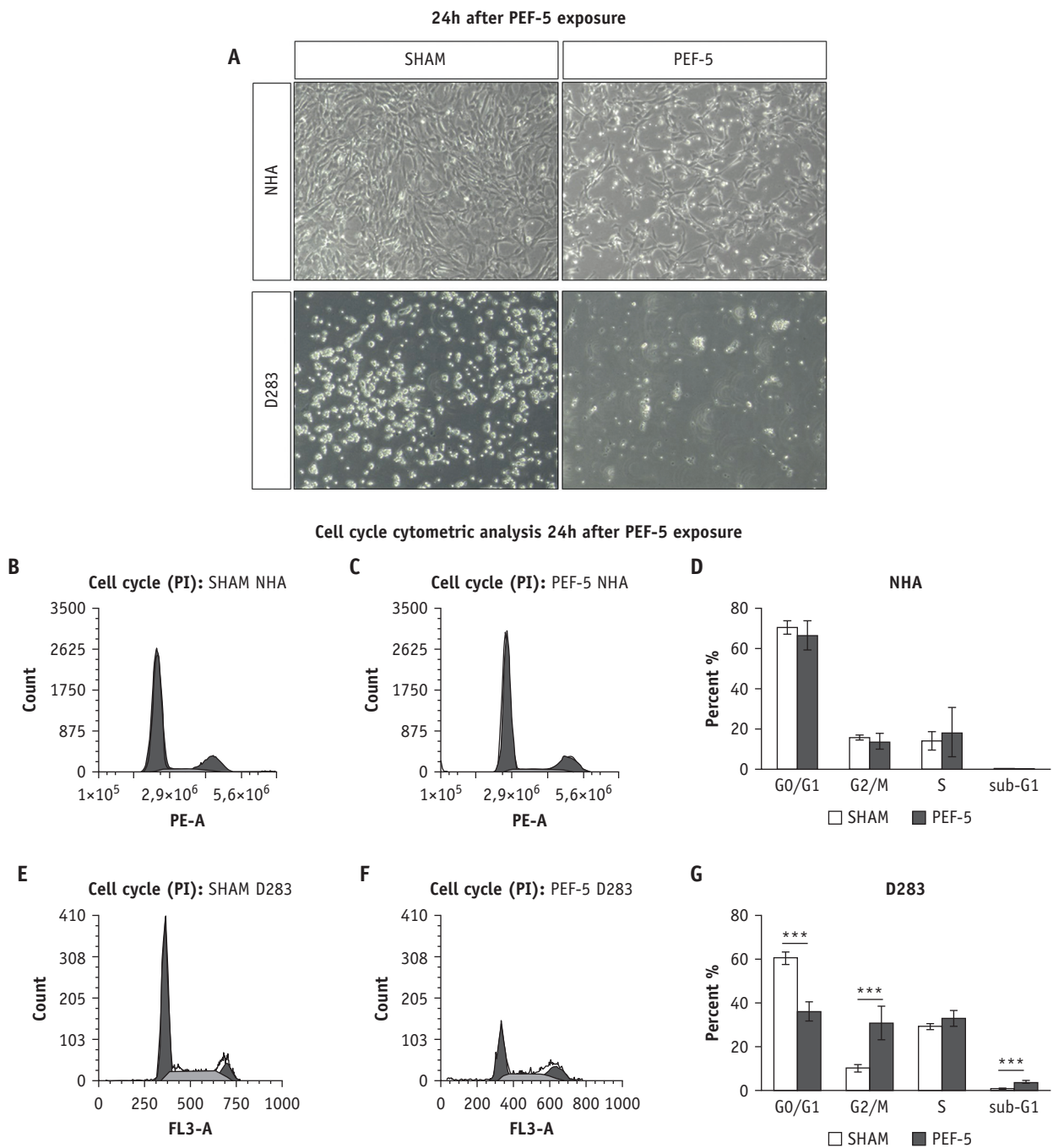


Fig. 2. Cell cycle perturbation after PEF-5 exposure. Representative images of D283 and normal human astrocytes (NHA) 24 hours after exposure (A). Histograms of cell cycle in NHA (B and C) and D283 (E and F) and associated bar graphs (D-G).

proliferation rate in D283 cells ($P = .0074$ and $P = .0070$), compared with 1.8- and 1.9-fold in NHAs ($P = .024$ and $P = .015$), respectively, 24 and 48 hours after the exposure.

PEF-5 induces perturbation in CSCs cell cycle

We analyzed the cell cycle status to assess the different impact of the electric exposure in terms of its perturbation in D283 and NHA.

In [Figure 2A](#), images of the 2 cell lines in normal conditions (left panels) and 24 hours after PEF-5 exposure (right panels) are reported. Analyzing the NHA cycle phase distribution ([Fig. 2B-D](#)), we did not find any significant differences between sham and exposed cells. Conversely, D283 cells showed a significant decrease in the G0/G1 phase (pulsed vs sham $P < .0001$), with a consequent significant increase in sub-G1 (pulsed vs sham $P < .0001$) and G2/M phase (pulsed vs sham $P = .0007$), suggesting consistent levels of cell death and a G2/M arrest of living cells ([Fig. 2E-G](#)).

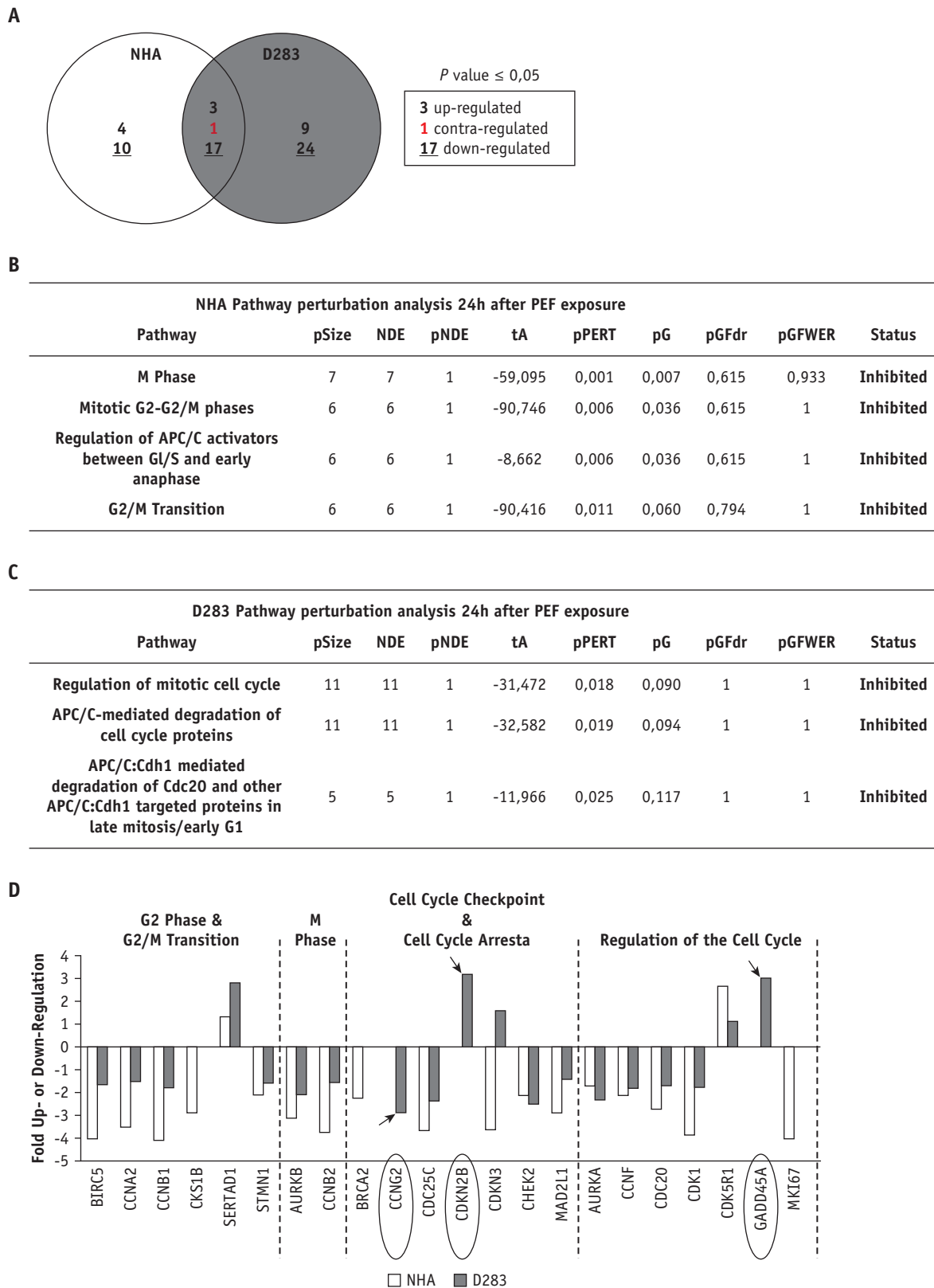


Fig. 3. Bioinformatics analysis. Venn diagram shows the number of common and exclusively deregulated genes in normal human astrocytes (NHA) and D283 (A). Pathway perturbations respectively in NHA (B) and D283 (C). pSize is the number of genes involved, tA is the perturbation score, pPERT is the bootstrap probability of pathway perturbation associated with tA and is considered significant at $P < .05$. Positive tA values indicate pathway activation, and negative values indicate inhibition. (D) The expression level of significantly deregulated genes 24 hours after exposure in D283 versus with NHA. Black arrows indicate deregulated genes exclusively in D283 cells.

PEF-5 causes G2/M arrest and activates apoptosis and senescence processes exclusively in CSCs

To evaluate the influence of PEF-5 on signaling pathways regulating cell division, we examined expression profiles of 84 genes with established roles. This analysis was carried out on both NHA and D283 cells 24 hours after exposure or sham-treatment. As shown in the Venn diagram (Fig. 3A), significantly deregulated genes are mostly downregulated in both cell lines. Of note, the number of significantly deregulated genes in D283 cells exceeds twice that of NHA (33/84 [39.3%] vs 14/84 [16.6%]), suggesting an important cell cycle perturbation induced by PEF-5 in CSCs with respect to normal cells. To identify the molecular mechanism regulating this different response, we performed an analysis of perturbed pathways using Signaling Protein Impact Analysis, starting from significantly deregulated genes in treated D283 and NHA, compared with ones obtained in untreated cells. As for NHAs, the analysis highlighted that M phase, mitotic G2-G2/M phases, regulation of APC/C activators between G1/S and early anaphase, and G2/M transition pathways were inhibited (Fig. 3B); hence, no specific cell cycle phase was perturbed after exposure. D283 cells pathway analysis instead showed inhibition in regulation of mitotic cell cycle, APC/C-mediated degradation of cell cycle proteins, APC/C:Cdh1-mediated degradation of Cdc20, and other APC/C:Cdh1-targeted proteins in late mitosis/early G1 pathways (Fig. 3C), according to flow cytometric data (Fig. 2 E-G).

The graph in Figure 3D shows the expression level of significantly deregulated genes 24 hours after exposure. We focused our attention on 3 genes exclusively deregulated in D283 cells: *CCNG2*, *CDKN2B*, and *GADD45A*. The downregulation of the *CCNG2* gene suggests a negative regulation of G1/S transition,³¹ and upregulation of *GADD45A* is reported to be associated with the G2 arrest³² in correlation with the upregulation of the *CDKN2B* gene. To verify the hypothesis that PEF-5-induced cell death and senescence could be mediated by *GADD45A*, we evaluated its expression levels in conjunction with those of cleaved-caspase-3 and p15 proteins, key mediators of apoptotic and senescence signaling, respectively. As shown in Figure 4, the expression kinetics revealed a statistically significant *GADD45A* expression level 3 hours after exposure (PEF-5 vs sham; $P = .0265$), consistent with the significant increase in cleaved-caspase-3 (PEF-5 vs sham; $P = .0010$) and p15 (PEF-5 vs sham; $P = .0017$) at a later time (ie, 24 hours after PEF-5 exposure).

Clonogenic survival assay after PEF-5 exposure and ionizing radiation combined treatment

As shown in Figure 5A and 5B, exposure to PEF-5 efficiently decreased the clonogenic capacity of D283 cells (4 times less than sham-treated cells; $P < .0041$). Thus, we tested a combined protocol of exposure, delivering

increasing ionizing radiation (IR) doses (2, 5, and 8 Gy) 3 hours after PEF-5 exposure, in conjunction with the highest found *GADD45A* protein expression level. The combined treatment of PEF-5 and IR was able to reduce clone formation significantly (Fig. 5A and 5B). Notably, PEF-5 exposure reduced clone formation with the same efficacy of the highest x-ray dose delivered, implying the possibility of using PEF-5 as a pretreatment to de-escalate IR doses.

PEF-5 and IR combined treatment inhibits the tumor growth in vivo

As previously demonstrated, subcutaneous implantation of 6×10^6 D283 cells in nude mice was sufficient to ensure 100% of tumor engraftment within 12 days postinjection.²⁰ To verify PEF-5's efficacy in modifying the tumorigenic potential of D283 cells, treated and sham-treated cells were implanted in the right flank of CD1 nude mice. PEF-5 exposure significantly delayed tumor growth compared with the sham group, with a final tumor growth inhibition (TGI%) of 46.47% at 43 days post-treatment, indicating that PEF-5 alone is sufficient to affect the tumor growth significantly (Fig. 5D and 5E).

We then tested a combined exposure protocol (PEF-5 + 2 Gy) to validate in vivo the sensitizing effect induced by PEF-5 pre-exposure in vitro. To this aim, mice were locally irradiated 3 hours after implantation of PEF-5 or sham-treated cells with 2 and 5 Gy of x-rays, respectively. As expected, IR alone (5 Gy) significantly inhibited tumor growth, reaching a TGI% value of 87.18% at 43 days post-treatment. Combined treatment (PEF-5 + 2 Gy) significantly inhibited tumor growth compared with the 5 Gy group (PEF-5 + 2 Gy vs 5 Gy alone; $P = .0061$), reaching a final TGI value of 100% with respect to the sham group (Fig. 5D and 5E). No tumor regrowth was observed in the PEF-5 + 2 Gy group up to 110 days post-treatment, suggesting complete tumor growth inhibition maintained over the long term. These data demonstrate the ability of μ sPEFs to act as a radiosensitizer enhancing the x-ray response in vivo.

Discussion

CSCs are strongly involved in the onset of cancer and constitute an endless reserve for tumor maintenance and progression. They also appear to be the reason why conventional therapies fail (ie, chemotherapy and radiation therapy) and the cause of cancer relapse and metastasis.¹⁵⁻¹⁷ Electrically mediated therapies are good candidates for new therapeutic strategies to specifically target CSCs,^{33,34} as well as to reduce or eliminate side effects associated with conventional therapies, although studies on this topic are still scarce.

Here, for the first time, we explored this hypothesis by taking advantage of a suitable biological cell model rich in CSCs. As recently demonstrated, D283 cells,

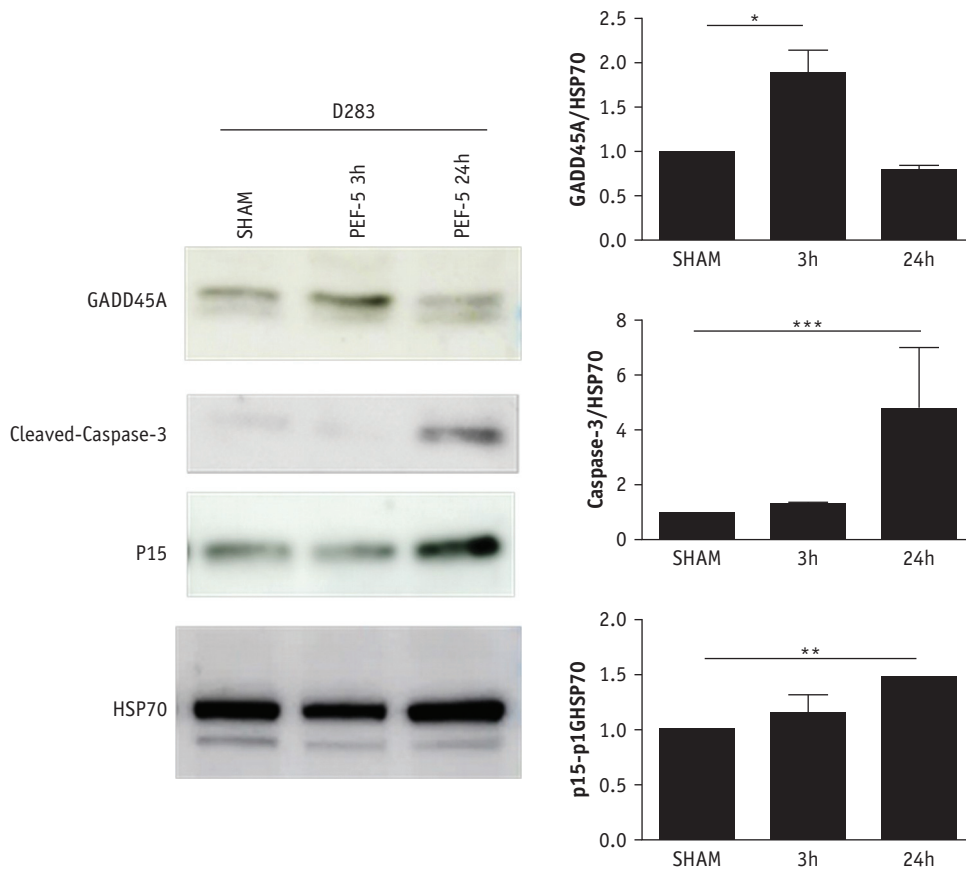


Fig. 4. Validation of protein expression of key genes suggested from the bioinformatics analysis. Western blot analysis of GADD45A, cleaved-caspase-3, and p15 (A) and densitometric analysis (B), evaluated 3 and 24 hours after D283 exposure.

representative of patient molecular subtypes 3/4, are characterized by an intrinsic ubiquitous expression of CD133, are extremely tumorigenic, and show peculiar dielectric characteristics.²³ We well characterized μ PEF action also on normal NHAs, these cells being located in the immediate surroundings of the tumor area and toward which any undesirable side effect induced by the electric treatment should be avoided.

We highlighted a selective action of PEF-5 exposure to irreversibly electroporate D283 cells but not NHA. We established the permeabilization threshold for D283 cells, in the case of both reversible and irreversible electroporation, as a function of the electric pulse number. Reversible electroporation is achievable when delivering to CSCs less than 5 electric pulses (at an amplitude of 0.3 MV/m lasting 40 μ s); higher than this pulse number, D283 cells start to experience irreversible electroporation with consequent high levels of cell death. Different behavior is observed in NHAs, which are reversibly electroporated also when 5 electric pulses are applied, suggesting that irreversible electroporation could be achievable when applying a higher number of electric pulses.

Similar behavior for NHAs exposed to a different μ PEF protocol has been reported in previous studies,^{33,34} in comparison with glioblastoma cancer stem-like cells. In

these studies, the role of cell dimension and aspect ratio between the cell nucleus and the cytoplasm diameters in regulating μ PEF's selective action on the glioblastoma CSCs were hypothesized and assessed. In our investigation, the selective action of μ PEF on MB cells seems to not depend on cell dimension and aspect ratio, as opposed to what has been reported elsewhere.³⁴ The more sensitive D283 cells are much smaller (diameter of about 10 μ m) than NHAs (diameter of about 20 μ m). This result is also in contrast to what is usually believed in electroporation theories and models,³⁵ suggesting that bigger cells should be electroporated more easily than smaller ones, hence presenting a higher electroporation threshold.³⁶

Therefore, other plausible mechanisms of selective μ PEF action on D283 cells should be taken into account; among many, one explanation may imply the modulation of intracellular events mediated by the transmembrane protein CD133,^{37,38} resulting in specific action of the electric exposure on MB CSCs rich in CD133 protein. With respect to this result, Song et al found that ablation of CD133 attenuated the capacity of defense against ROS in hepatocellular cancer cells through decreasing glutathione levels,³⁹ indicating a functional role for CD133 in ROS defense and in evading anticancer therapies. Therefore, possible μ PEF-mediated CD133 dysfunction could

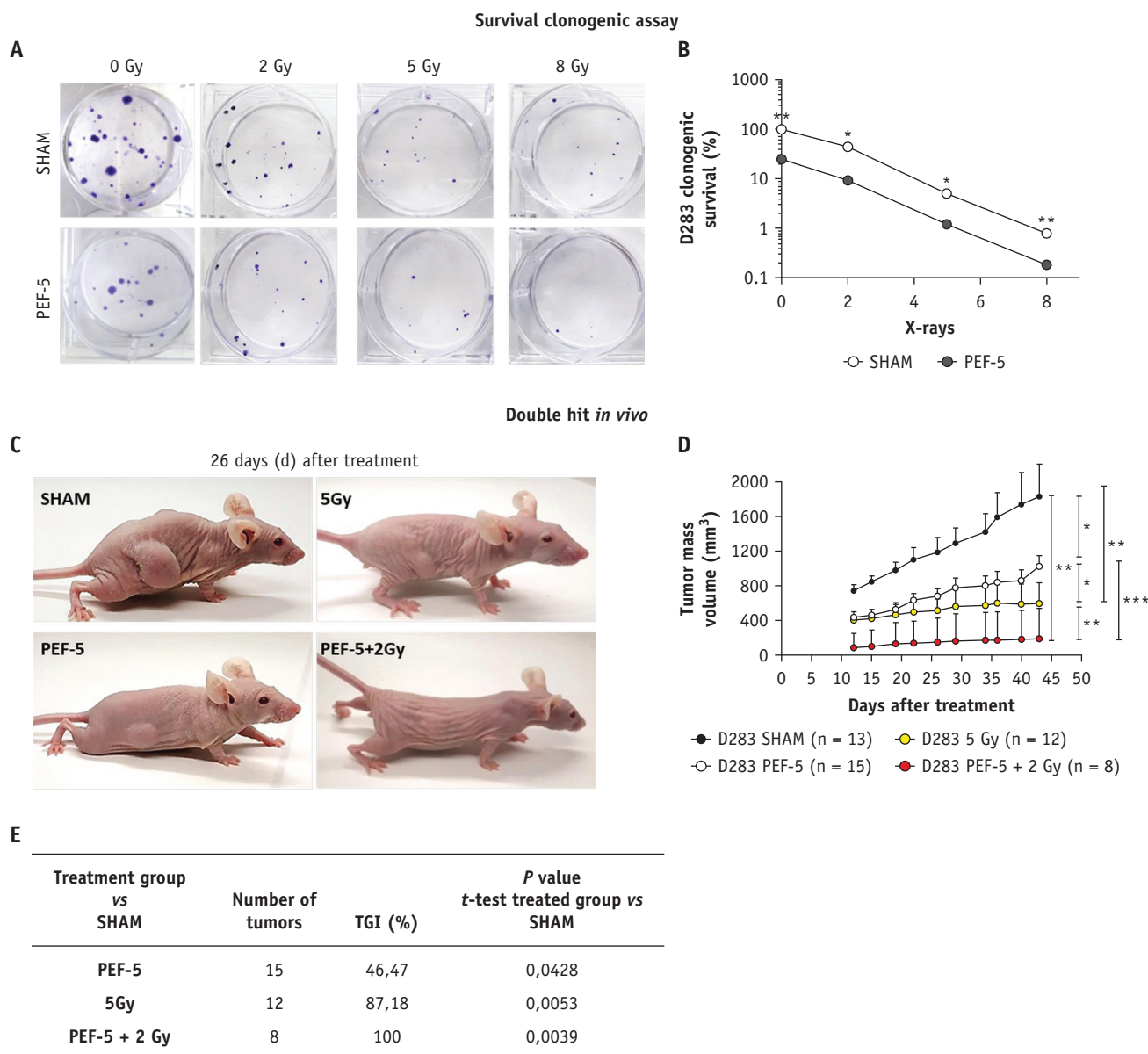


Fig. 5. Survival clonogenic assay in vitro and tumor growth in vivo. Images of clonogenic survival of D283 after exposure and ionizing radiation combined treatment (A) and associated graph (B); the curves represent the average of 2 independent experiments. Images of tumor masses with different dimension at 26 days postimplantation (C). Tumor-propagating capacity of each treated group (D). TGI% of treated tumors for each experimental group (E).

amplify ROS generation, as shown in our data 3 hours postexposure, and their action could selectively influence the final cell fate.

Globally, the specific membrane compositions and complexity could make the difference, enabling a peculiar molecular cell response to electric exposure, the cell membrane being the main μ PEF target.^{1,2,5,7,35} The differential response could be related to different membrane structures in terms of phospholipids, transmembrane proteins (eg, membrane channels, cytoskeleton), enzymes, and/or receptors that can respond or be activated differently depending on their specific expression and the different cell types.⁴⁰ This hypothesis implies that biological and

specifically molecular processes are primary mediators of the cell response to μ PEF and should be investigated much more deeply to effectively understand the reason of for such selectivity, also in relation to biophysical (electroporation and electropermeabilization of cell membranes) and/or biochemical (eg, lipid peroxidation) processes.¹

In our understanding, ROS generation after μ PEF exposure in surviving D283 cells could be considered one of the steps in this process; ROS are ubiquitous second messengers regulating cell growth, differentiation, progression, and death.⁴¹ It has already been reported that the redox scavenger system is strongly activated in CSCs and that this activation contributes to the maintenance of lower

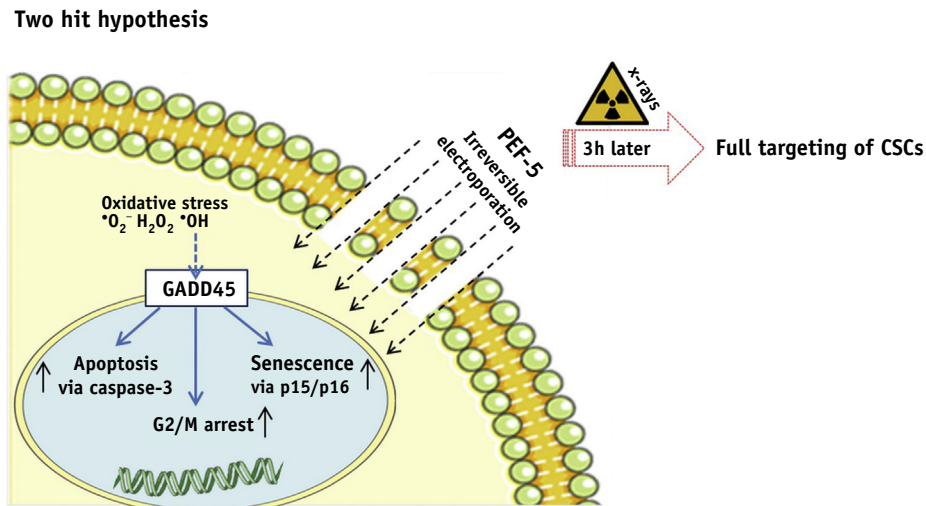


Fig. 6. Mechanism sketch of the multimodal treatment to target cancer stem cells (CSCs). A conclusive summary of the mechanisms highlighted in this work for the combined μ sPEF and ionizing radiation (IR) treatments to target CSCs. IR applied 3 hours after μ sPEF exposure amplified cell alterations in terms of reactive oxygen species, apoptosis, senescence, and proliferation arrest, triggering definitive defeat of CSCs.

ROS levels in CSCs, compared with those in non-CSCs, in various cancer types.⁴² Hence, on one hand, ROS generation activated by μ sPEF could determine a direct action on DNA damage to enable D283 cell radiosensitization,⁴³ On the other hand, the μ sPEF effect, inducing temporary enhancement of ROS in surviving CSCs, could be responsible for the initiation of the observed D283 proliferation inhibition and reduction of clonogenic survival. Indeed, in this indirect mechanism of radiosensitization, ROS may activate p38 MAPK and JNK transduction pathways, as reported in the study by Son et al,⁴⁴ recognized to mediate GADD45A expression to direct cells toward apoptosis or senescence.

In our study, x-rays were delivered specifically after 3 hours from the electric exposure in correspondence to the maximal expression of the GADD45A protein. If the accumulated damage cannot be repaired, cells will undergo apoptosis,⁴⁵ as shown by the upregulation of cleaved-caspase-3 24 hours after μ sPEFs exposure. Furthermore, senescence commitment via p15/p16 upregulation achieved 24 hours after μ sPEFs exposure was established. Senescent cells fail to proliferate but remain metabolically active⁴⁶ in a dynamic process.⁴⁷ In a recent paper, some authors support the idea that senescence evasion is necessary and that it is a hallmark for SHH MB progression driving p53 inactivation.⁴⁸ Hence, PEF-5 exposure could commit cells in a senescence state or in G2/M arrest, making them more prone to death when a second hit (x-rays) arrives to definitively defeat CSCs.

GADD45A has been shown to mediate the activation of several molecules (eg, MTK1/MEKK4, p38, JNK, NFkB, CDK1/Cyclin B1, and p53) involved in the regulation of many cellular functions, including cell cycle arrest, DNA repair, and apoptosis, and to be involved in crucial steps in

tumor growth suppression. In particular, according to the literature,⁴⁵ GADD45A could sensitize MB cells for future treatments, such as irradiation, inducing arrest in G2/M phase of the cell cycle. As the p53 downstream gene, GADD45A is involved in the control of the G2-M checkpoint, through a mechanism that remains poorly understood. However, many of the G2-M regulators appear to ultimately target CDC2/cyclin B1, a protein kinase required for mitotic entry in mammalian cells. According to our results, overexpression of different isoforms of GADD45 blocks cell proliferation.⁴⁹ These findings suggest that pulsed electric exposure may play an important role in sensitizing CSCs, also blocking their proliferation capacity and hence possibly promoting a stronger action with x-rays on the pretreated D283 cells.

Because one of the main demands in MB treatment is the ability to deliver reduced IR doses to limit cognitive side effects, in the present study we investigated the possibility of radiosensitization induced by the μ sPEF pretreatment on D283 cells. Remarkably, we demonstrated *in vivo* that a combined treatment completely inhibited tumor growth, which represents an interesting therapeutic strategy to selectively target CSCs, safeguarding the healthy tissues and overcoming radiation therapy-associated cognitive disabilities typically associated with brain tumor therapies.⁵⁰ Our investigation is a first and indispensable step toward this further verification.

The possible role of the microenvironment (eg, local inflammation and modification of tumor vasculature) in the synergy between the 2 physical agents and the activation of immunogenic responses and inflammation are other important aspects to be assessed. In particular, μ sPEF exposure can activate targets of immune response (as damage-associated molecular patterns), accumulation of

inflammatory cells, and immune cytokines,^{11,12} which deserve investigation in a forthcoming *in vivo* study.

Conclusions

Our data seem to support a D283-selective alteration under PEF-5 and IR combined exposure as summarized in Figure 6, outlining this new therapeutic strategy to selectively eradicate the more resistant CSCs.

References

- Kotnik T, Rems L, Tarek M, et al. Membrane electroporation and electropermeabilization: Mechanisms and models. *Annu Rev Biophys* 2019;48:63-91.
- Gothelf A, Mir LM, Gehl J. Electrochemotherapy: Results of cancer treatment using enhanced delivery of bleomycin by electroporation. *Cancer Treat Rev* 2003;29:371-387.
- Daud AI, De Conti RC, Andrews S, et al. Phase I trial of interleukin-12 plasmid electroporation in patients with metastatic melanoma. *J Clin Oncol* 2008;26:5896-5903.
- Marty M, Sersa G, Garbay JR, et al. Electrochemotherapy—An easy, highly effective and safe treatment of cutaneous and subcutaneous metastases: Results of ESOPE (European Standard Operating Procedures of Electrochemotherapy) study. *EJC Suppl* 2006;4:3-13.
- Gehl J, Sersa G, Wichmann Matthiessen L, et al. Updated standard operating procedures for electrochemotherapy of cutaneous tumors and skin metastases. *Acta Oncol* 2018;57:874-882.
- Cornelis FH, Ben Ammar M, Nouri-Neuville M, et al. Percutaneous image-guided electrochemotherapy of spine metastases: Initial experience. *Cardiovasc Intervent Radiol* 2019;42:1806-1809.
- Davalos RV, Mir LM, Rubinsky B. Tissue ablation with irreversible electroporation. *Ann Biomed Eng* 2005;33:223-231.
- Sano MB, Arena CB, Bittleman KR, et al. Bursts of bipolar microsecond pulses inhibit tumor growth. *Sci Rep* 2015;5:14999.
- Simon CJ, Dupuy DE, Mayo-Smith WW. Microwave ablation: Principles and applications. *Radiographics* 2005;25(suppl 1):S69-S83.
- Scheffer HJ, Nielsen K, de Jong MC, et al. Irreversible electroporation for nonthermal tumor ablation in the clinical setting: A systematic review of safety and efficacy. *J Vasc Intervent Radiol* 2014;25:997-1011.
- Rigel-Scaia VM, Beitel-White N, Lorenzo MF, et al. High-frequency irreversible electroporation is an effective tumor ablation strategy that induces immunologic cell death and promotes systemic anti-tumor immunity. *EBioMedicine* 2019;44:112-125.
- Calvet C, Mir LM. The promising alliance of anti-cancer electrochemotherapy with immunotherapy. *Canc Metastasis Rev* 2016;35:165-177.
- Zhao J, Wen X, Tian L, et al. Irreversible electroporation reverses resistance to immune checkpoint blockade in pancreatic cancer. *Nat Commun* 2019;10:899.
- Jordan CT, Guzman ML, Noble M. Cancer stem cells. *N Engl J Med* 2006;355:1253-1261.
- Singh SK, Clarke ID, Terasaki M, et al. Identification of a cancer stem cell in human brain tumors. *Cancer Res* 2003;63:5821-5828.
- Reya T, Morrison SJ, Clarke MF, et al. Stem cells, cancer, and cancer stem cells. *Nature* 2001;414:105-111.
- Ayob AZ, Ramasamy TS. Cancer stem cells as key drivers of tumour progression. *J Biomed Sci* 2018;25:20.
- Louis DN, Perry A, Reifenberg G, et al. The 2016 World Health Organization classification of tumors of the central nervous system: A summary. *Acta Neuropathol* 2016;131:803-820.
- Smoll NR, Drummond KJ. The incidence of medulloblastomas and primitive neuroectodermal tumours in adults and children. *J Clin Neurosci* 2012;19:1541-1544.
- Casciati A, Tanori M, Manczak R, et al. Human medulloblastoma cell lines: Investigating on cancer stem cell-like phenotype. *Cancers* 2020;12:226.
- Davis IW, Merla C, Casciati A, et al. Push-pull configuration of high-power MOSFETs for generation of nanosecond pulses for electropermeabilization of cells. *Int J Microw Wirel Technol* 2019;11:645-657.
- Kanaan M, Amari S, Silve A, et al. Characterization of a 50-Ω exposure setup for high-voltage nanosecond pulsed electric field bio-experiments. *IEEE Trans Biomed Eng* 2011;58:207-214.
- Merla C, Liberti M, Marracino P, et al. A wide-band bio-chip for real-time optical detection of bioelectromagnetic interactions with cells. *Sci Rep* 2018;8:5044.
- Merla C, Liberti M, Consales C, et al. Evidences of plasma membrane-mediated ROS generation upon ELF exposure in neuroblastoma cells supported by a computational multiscale approach. *Biochim Biophys Acta Biomembr* 2019;1861:1446-1457.
- Nuccitelli R, Lui K, Kreis M, et al. Nanosecond pulsed electric field stimulation of reactive oxygen species in human pancreatic cancer cells is Ca²⁺-dependent. *Biochem Biophys Res Commun* 2013;435:580-585.
- Tanori M, Pannicelli A, Pasquali E et al. Cancer risk from low dose radiation in Ptch1+/- mice with inactive DNA repair systems: Therapeutic implications for medulloblastoma. *DNA Repair* 2019;74:70-79.
- Bai L, Zhou B, Yang CY, et al. Targeted degradation of BET proteins in triple-negative breast cancer. *Cancer Res* 2017;77:2476-2487.
- Berardinelli F, Tanori M, Muoio D, et al. G-quadruplex ligand RHPS4 radiosensitizes glioblastoma xenograft *in vivo* through a differential targeting of bulky differentiated- and stem-cancer cells. *J Exp Clin Cancer Res* 2019;38:311.
- Bonnafeus P, Vernhes MC, Teissie J, et al. The generation of reactive-oxygen species associated with long-lasting pulse-induced electropermeabilisation of mammalian cells is based on a non-destructive alteration of the plasma membrane. *Biochim Biophys Acta* 1999;46:123-134.
- Ryu JM, Lee HJ, Yung YH, et al. Regulation of stem cell fate by ROS-mediated alteration of metabolism. *Int J Stem Cells* 2015;8:24-35.
- Faradji F, Bloyer S, Dardalhon-Cuménal D, et al. Drosophila melanogaster cyclin G coordinates cell growth and cell proliferation. *Cell Cycle* 2011;10:805-818.
- Wang XW, Zhan Q, Coursen JD, et al. GADD45 induction of a G2/M cell cycle checkpoint. *Proc Natl Acad Sci U S A* 1999;96:3706-3711.
- Rolong A, Schmelz EM, Davalos RV. High-frequency irreversible electroporation targets resilient tumor-initiating cells in ovarian cancer. *Integr Biol (Camb)* 2017;9:979-987.
- Ivey JW, Wasson EM, Alinezhadbalalami N, et al. Characterization of ablation thresholds for 3D-cultured patient-derived glioma stem cells in response to high-frequency irreversible electroporation. *Research (Wash D C)* 2019;2019:8081315.
- Kotnik T, Miklavcic D. Analytical description of transmembrane voltage induced by electric fields on spheroidal cells. *Biophys J* 2000;79:670-679.
- Agarwal A, Zudans I, Weber EA, et al. Effect of cell size and shape on single-cell electroporation. *Anal Chem* 2007;79:3589-3596.
- Sui X, Chen R, Wang Z, et al. Autophagy and chemotherapy resistance: A promising therapeutic target for cancer treatment. *Cell Death Dis* 2013;4:e838.
- Rappa G, Fargeas CA, Le TT, et al. Letter to the editor: An intriguing relationship between lipid droplets, cholesterol-binding protein CD133 and Wnt/β-catenin signaling pathway in carcinogenesis. *Stem Cells* 2015;33:1366-1370.
- Song Y, Jang J, Shin T-H, et al. Sulfasalazine attenuates evading anticancer response of CD133-positive hepatocellular carcinoma cells. *J Exp Clin Cancer Res* 2017;36:38.
- Hoejholt KL, Muzic T, Jensen SD, et al. Calcium electroporation and electrochemotherapy for cancer treatment: Importance of cell

- membrane composition investigated by lipidomics, calorimetry and in vitro efficacy. *Sci Rep* 2019;9:4758.
41. Zhang H, Gomez AM, Wang X, et al. ROS regulation of microdomain Ca^{2+} signalling at the dyads. *Cardiovasc Res* 2013;98:248-258.
 42. Shi XK, Zhang Y, Zheng JH, et al. Reactive oxygen species in cancer stem cells. *Antioxid Redox Signal* 2012;16:1215-1228.
 43. Jiang J, Wang H, De Ridder M. Targeting antioxidant enzymes as a radiosensitizing strategy. *Cancer Lett* 2018;348:154-164.
 44. Son Y, Cheong Y-K, Kim N-H, et al. Mitogen-activated protein kinases and reactive oxygen species: How can ROS activate MAPK pathways? *J Signal Transduct* 2011;2011:792639.
 45. Tamura E, de Vasconcellos F, Sarkar D, et al. GADD45 proteins: Central players in tumorigenesis. *Curr Mol Med* 2012;12:634-651.
 46. Smith MA, Peeper DS. Epithelial-mesenchymal transition and senescence: Two cancer-related processes are crossing paths. *Aging (Albany NY)* 2010;2:735-741.
 47. Lee S, Schmitt CA. The dynamic nature of senescence in cancer. *Nat Cell Biol* 2019;21:94-101.
 48. Tamayo-Orrego L, Swikerta SM, Charrona F. Evasion of cell senescence in SHH medulloblastoma. *Cell Cycle* 2016;15:2102-2107.
 49. Zhang L, Yang Z, Liu Y. GADD45 proteins: Roles in cellular senescence and tumor development. *Exp Biol Med (Maywood)* 2014;239:773-778.
 50. Makale MT, McDonald CR, Hattangadi-Gluth JA, et al. Mechanisms of radiotherapy-associated cognitive disability in patients with brain tumours. *Nat Rev Neurol* 2017;13:5264.